33
Research paper
Doi 10.61892/stp202401015M
ISSN 2566-4484

Dragan Milašinović, University of Novi Sad, ddmilasinovic@gmail.com
Nataša Mrđa Bošnjak, University of Banja Luka, natasa.mrdja-bosnjak@aggf.unibl.org

MODELING OF POROUS DRY MATERIALS USING RHEOLOGICAL-DYNAMICAL ANALOGY

Abstract

A theoretical model for porous viscoelastoplastic (VEP) materials under dry conditions is examined based on the principles of mass and energy conservation using rheological-dynamical analogy (RDA). The model provides the expressions for the creep coefficient, Poisson's ratio, modulus of elasticity, damage variable and strength in the function of porosity and/or void volume fraction (VVF). Compared with numerous versions of acoustic emission monitoring developed to analyze the behavior of the total wave propagation in inhomogeneous media with density variation, the RDA model is found to be comprehensive in interpretation and consistent with physical understanding. The reliability of the proposed model is confirmed by the comparison of numerical results with experimental ones on hardened concrete and rocks.

Keywords: porosity, RDA model, wave propagation, density variation, creep effects, cracks

МОДЕЛИРАЊЕ ПОРОЗНИХ МАТЕРИЈАЛА У СУВОМ СТАЊУ РЕОЛОШКО – ДИНАМИЧКОМ АНАЛОГИЈОМ

Сажетак

Теоријски модел за порозне вискоеластопластичне (VEP) материјале у сувом стању је испитан на основу принципа очувања масе и енергије примјеном реолошко – динамичке аналогије (RDA). Модел даје изразе за коефицијент течења, Поасонов коефицијент, модул еластичности, варијаблу оштећења и чврстоћу у функцији порозности и/или запреминског удјела празнина (VVF). У поређењу са бројним верзијама праћења акустичне емисије развијеним за анализу понашања укупног ширења таласа у нехомогеним медијима са варијацијама густине, RDA модел је свеобухватан у интерпретацији и конзистентан са физичким разумјевањем. Поузданост предложеног модела потврђује поређење нумеричких резултата са експерименталним на очврслим бетонима и стенама.

Кључне ријечи: порозност, RDA модел, пропагација таласа, паријација густине, ефекти течења, пукотине

1. INTRODUCTION

So far, many relationships have been established between porosity and key mechanical properties such as strength and modulus of elasticity. However, the utility and physical significance of many of these relationships are often unclear as most theoretical models are based on some idealized physical microstructure, and the resulting correlations often cannot be applied to actual materials and practical applications, [1]. Spriggs's empirical equation for Young's modulus of porous materials [2], and the similar Ryshkewitch-Duckworth [3] equation for the strength of porous materials have long been accepted by the literature. Phani and Niyogi [4] derived a semi-empirical equation to describe the porosity dependence of Young's modulus of brittle solids. Wang [5] obtained theoretically the relationship between Young's modulus and porosity of porous alumina, in situations where the porosity percentage not only changes, but changes also occur from interconnected to disconnected pore structures. The dependence applies to the entire range of porosity and can treat the transition of the pore structure from interconnected to isolated. However, later, advances in predicting the elastic properties of porous materials over the entire porosity range were closely related to the relationship to Phani and Niyogi [4].

One of the most important factors that determine the mechanical properties of hardened concrete is its porosity, as well as the number, size, and interconnection of pores in hardened cement paste, [6]. Many proposed expressions can be found in the literature that establish the relationship between the porosity of hardened concrete and its mechanical properties - compressive strength and modulus of elasticity, [7], [8], [9], [10]. These connections are most often established by applying statistical processing of experimentally determined data on a limited number of samples of certain characteristics, and their accuracy in practical application is conditioned by the similarity of real concrete with these samples.

Rock porosity varies in a wide range. Theories for the poroelastic behavior of rocks can be developed based on two conceptual models of porous rock: a solid material permeated with an interconnected collection of voids [11] or aggregation of grains in partial contact with each other at various points [12]. The latter model is more appropriate for soils, whereas the former has proven to be more fruitful for studying rocks. An additional difficulty in establishing the relationship between porosity and mechanical properties of rocks is obtaining reliable data on the porosity in the rock masses, which usually are based on testing samples (e.g., using the method of porosimetry by mercury injection) taken from selected sites.

The main goal of this paper is to analyze predicted relationship form [13] between mechanical parameters and VVF of damaged materials. In this paper, it is considered that the principles of conservation of mass and energy are valid for wave motion between two cross-sections of the sample, regardless of how the material behaves in terms of the size and distribution of material particles. Damage evolution is considered to be an increase in degradation of material properties compared to their initial states due to the change of VVF.

2. DESCRIPTION OF MODEL PARAMETERS

The relationship between the creep coefficient and Poisson's ratio is given in [14]

$$\varphi = \frac{2\mu}{1-2\mu} \tag{2}$$

In the wave motion, a very short time T^D is, due to which the creep coefficient is converted into a quotient of two moduli

$$\varphi = \frac{E_H}{E_K} \tag{3}$$

Where E_H is elastic modulus and E_K is the viscoelastic (VE) modulus.

According to [15], [13] the linear dependence of creep coefficient as a function of porosity is proposed in a form

$$\varphi(p) = \varphi_1 - \frac{p(\varphi_1 - \varphi_E)}{p_E} \tag{4}$$

where φ_1 is at zero porosity, while φ_E is at the end of the porosity interval [0, p_E]. p_E is defined at the end of measurable porosity. On the other hand, due to points (p_E, φ_E) and $(p_{max}, 0)$, the creep coefficient φ_E is

$$\varphi_E = \varphi_1 \left(1 - \frac{p_E}{p_{max}}\right) \tag{5}$$

The creep coefficient is a linear function of the modulus of elasticity, while the VE modulus is independent of porosity as a consequence of the principle of mass conservation. Consequently, Eq. (3) implies the linear relationship between the modulus of elasticity and porosity.

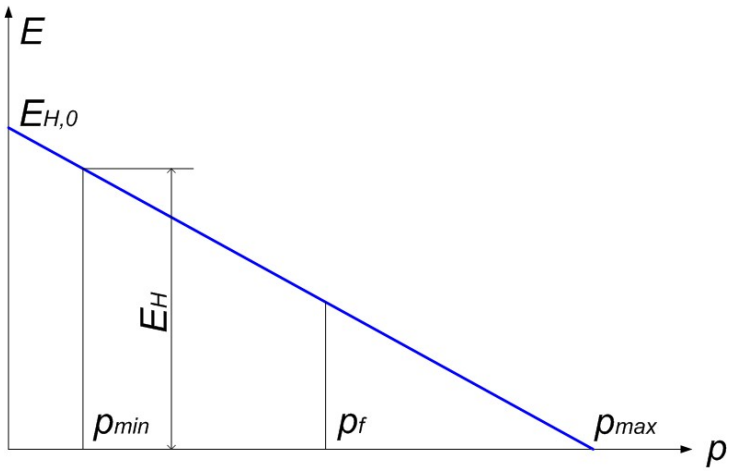

Figure 1. Young's modulus as a function of porosity.

According to the RDA model, the relationship between the Poisson's ratio and porosity for the interval [0, p_E] is

$$\mu_{RDA}(p) = \left[\varphi_1 - \frac{p(\varphi_1 - \varphi_E)}{p_E}\right] \Bigg/ \left\{2\left[1 + \varphi_1 - \frac{p(\varphi_1 - \varphi_E)}{p_E}\right]\right\} \tag{6}$$

The dynamic Poisson's ratio of solid material in its initial state can be obtained using the P and S wave velocities

$$\mu_1 = \frac{v_L^2 - 2v_T^2}{2\left(v_L^2 - v_T^2\right)} \tag{7}$$

where v_L and v_T are the velocities of the P and S waves of a solid material in its initial state.

According to [14], the scalar damage variable of VEP material for the interval [0, p_E] is

$$\frac{\varphi_1}{1+\varphi_1} \geq D \geq \frac{\varphi_E}{1+\varphi_E} \tag{8}$$

where the initial (critical [16]) damage variable D_1 at zero porosity corresponds to the creep coefficient φ_1. Consequently, the nonlinear relationship between the damage variable and porosity is

$$D(p) = \left[\varphi_1 - \frac{p(\varphi_1 - \varphi_E)}{p_E}\right] \Bigg/ \left\{1 + \left[\varphi_1 - \frac{p(\varphi_1 - \varphi_E)}{p_E}\right]\right\}. \tag{9}$$

3. VOID VOLUME FRACTION

The solution of the quadratic equation derived by Milašinović et al. [17] are two values of Poisson's ratio

$$\mu_{1/2} = \frac{(\psi - 1) \pm \sqrt{\psi^2 - 10\psi + 9}}{4} \tag{10}$$

where Ψ is the ratio of the modulus of elasticity and dynamic modulus

$$\Psi = \frac{E_H}{E_D} \tag{11}$$

Based on two Poisson's ratios, the two stress-strain curves are obtained in [18], and they are:

$$\sigma_i = \frac{1}{2K_{E,i}}\left(\sqrt{1 + 4K_{E,i}E_i(0)\varepsilon} - 1\right), \quad i = 1,\ 2, \tag{12}$$

where

$$K_{E,i} = \frac{\varphi_i}{\sigma_{ef}}, \quad \varphi_i = \frac{2\mu_i}{1 - 2\mu_i}, \quad E_i(0) = E_H(1 + \varphi_i), \qquad i = 1,\ 2, \tag{13}$$

The effective stress σ_{ef} can be understood to represent not only the effect of reducing the geometric cross-section area due to damage, but also includes the effects of stress concentration in voids or the effects of interaction between voids, [19]

$$\sigma_{ef} = \frac{f_{cS}}{1 - D_1}, \tag{14}$$

where f_{cS} is the uniaxial unconfined compressive strength (UCS) of the damaged dry sample.

The damage state of ductile or VEP materials can be described by the VVF, [19]–[21]. The VVF is given by

$$VVF = \frac{dV - dV_0}{dV}, \tag{15}$$

where dV is the volume of a representative volume element (RVE) at a point in a material, while dV_0 is the volume of the matrix of RVE. It has been observed that the voids start to coalesce when they have grown to a size as large as the distance between them, [22], and the VVF at that stage is in the range of 0.15 through 0.25, [23].

Although Eq. (15) represents the definition of porosity, direct measurement of VVF is difficult. Because of that, it is rather easy to measure the density change of the material

$$VVF = 1 - \frac{\rho}{\rho_0}, \tag{16}$$

where the initial and the damage density of the material are denoted by ρ_0 and ρ.

Lemaitre and Dufailly [24] used the density change between the damaged and the initial state in interpreting the micromechanical model of a spherical void in a spherical RVE to prove the relation between the damage variable and porosity

$$D_{LD} = \left(1 - \frac{\rho}{\rho_0}\right)^{2/3}. \tag{17}$$

This is the relation between the surface damage and the variation of density or porosity.

In [13], Milašinović gave a detailed explanation of the limit values of VVF based on the strain energy densities shown in Figure 2, where

$$W_{el} = \frac{1}{2E_H}\sigma_{ef}^2,$$

$$\begin{aligned} W_{d1} &= \int_0^{\varepsilon_{cF}} \sigma_1 d\varepsilon = \int_0^{\varepsilon_{cF}} \frac{1}{2K_{E1}}\left(\sqrt{1+4K_{E1}E_1(0)\varepsilon}-1\right)d\varepsilon = \\ &= \frac{1}{2K_{E1}}\left[-\varepsilon_{cF} + \frac{-1+\left(1+4K_{E1}E_1(0)\varepsilon_{cF}\right)^{3/2}}{6K_{E1}E_1(0)}\right], \end{aligned} \tag{18}$$

$$\begin{aligned} W_{d2} &= \int_0^{\varepsilon_{cF}} \sigma_2 d\varepsilon = \int_0^{\varepsilon_{cF}} \frac{1}{2K_{E2}}\left(\sqrt{1+4K_{E2}E_2(0)\varepsilon}-1\right)d\varepsilon = \\ &= \frac{1}{2K_{E2}}\left[-\varepsilon_{cF} + \frac{-1+\left(1+4K_{E2}E_2(0)\varepsilon_{cF}\right)^{3/2}}{6K_{E2}E_2(0)}\right]. \end{aligned}$$

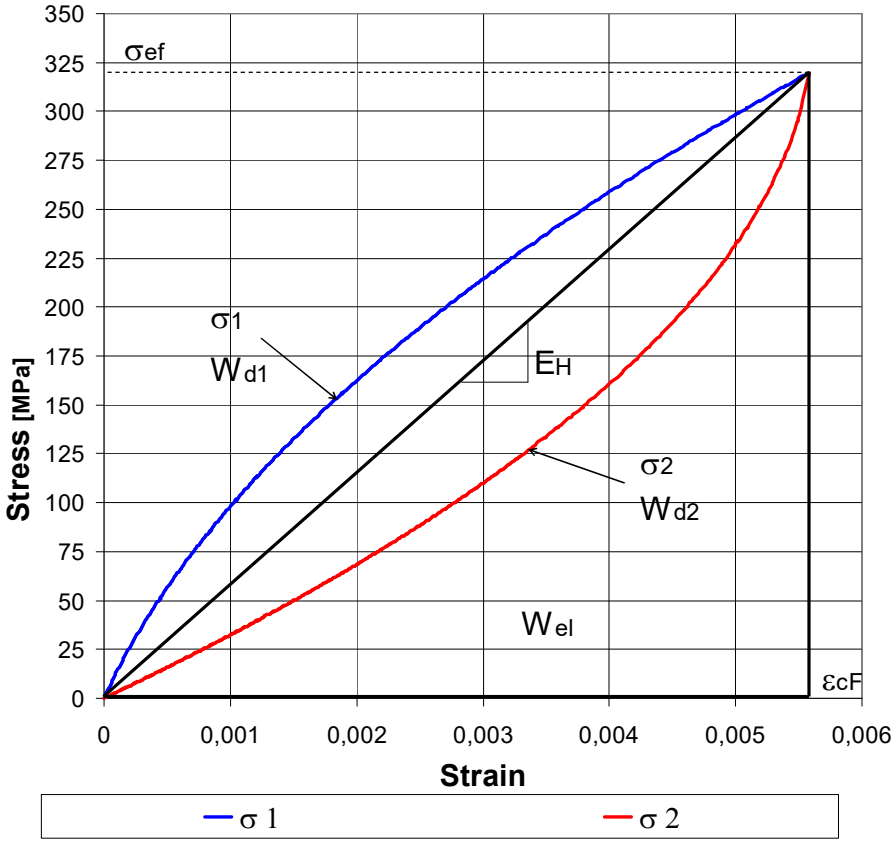

Figure 2. Strain energy densities: with positive Poisson's ratio (blue line) and with negative (red line)

The total energy density dissipation is

$$W_d = W_{d1} - W_{d2} \tag{19}$$

Consequently, the maximum VVF can be determined as follows

$$p_{max} = \frac{W_d}{W_{el}} = \frac{W_{d1} - W_{d2}}{W_{el}} . \tag{20}$$

It is well known that a positive Poisson's ratio is a measurable value, and a negative one is not. This fact allows us to determine the limit of measurable VVF

$$p_E = \frac{W_{d1} - W_{el}}{W_{el}} . \tag{21}$$

Using the difference between the W_{d1} and W_{d2} in relation to the W_d, the VVF which controls the macroscopic failure of the sample by the static strength f_{US2} [18] is

$$p_f = \frac{2W_{el} - W_{d1} - W_{d2}}{W_d} . \tag{22}$$

The previous difference in relation to the W_{el}, defines the minimum VVF which controls the dynamic strength f_{US1}

$$p_{min} = \frac{2W_{el} - W_{d1} - W_{d2}}{W_{el}} . \tag{23}$$

In [25] the relationship between the strength and the stress at the limit of elasticity is determined

$$\frac{\sigma_E}{f_{cS}} = \frac{\varphi_1}{1+\varphi_1} = D_1 . \tag{24}$$

So, the nonlinear relationship between the strength and VVF of dry VEP material denoted by according to [13] is

$$\sigma_f = \sigma_{ef} \left\{ 1 - \frac{p_f}{p_E} \left[1 - D_1 \left(1 - D_f \right) \right] \right\} . \tag{25}$$

4. ANALYSIS OF POROUS CONCRETE SAMPLES

A large number of experiments have shown that the elastic properties of wet concrete are affected by the degree of saturation, and that the strength of saturated concrete decreases, while the static and dynamic moduli of saturated concrete increase, [26], [27]. Experimental data from [26] were obtained on concrete samples with different amounts of entrained air and different water-cement ratios. A total of 15 samples were analyzed, some with very similar data. Therefore, only eight samples shown in [13], whose data are sufficiently different, were selected for this analysis.
According to [26] the average modulus of elasticity of the dry sample with zero porosity is $E_{H,0} = 45,35GPa$. Experimental results for eight selected samples are in detail analyzed in [13].
Assuming a linear change of modulus of elasticity with porosity in the interval [0, p_{max} = 0.508], where p_{max} is obtained for the sample No. 1 (35-00-L-2), we get the line shown in Figure 3, marked with black color. Figure 3 shows a comparison of the dimensionless moduli of elasticity obtained experimentally and by the RDA method. An excellent agreement of the results is observed.

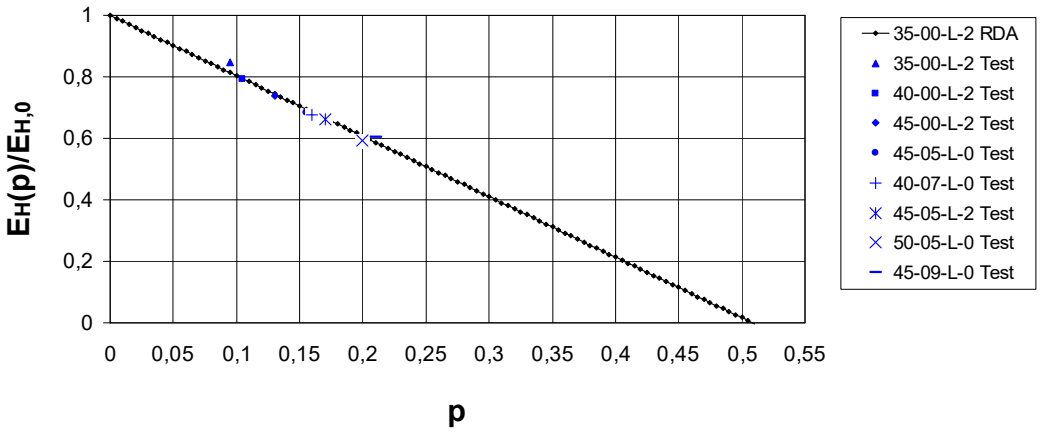

Figure 3. Comparisons of tested moduli of elasticity with functional dependence of modulus of elasticity versus porosity for sample No. 1 (35-00-L-2) according to RDA model

The calculated parameters by the RDA model associated with positive and negative values of Poisson's ratio are given in [13]. The functional dependence of the Poisson's ratio in relation to the porosity is shown in Figure 4 for sample No. 1 (35-00-L-2). The figure also shows a comparison of tested (μ) and numerically calculated (μ_1) values of Poisson's ratios that differ significantly.

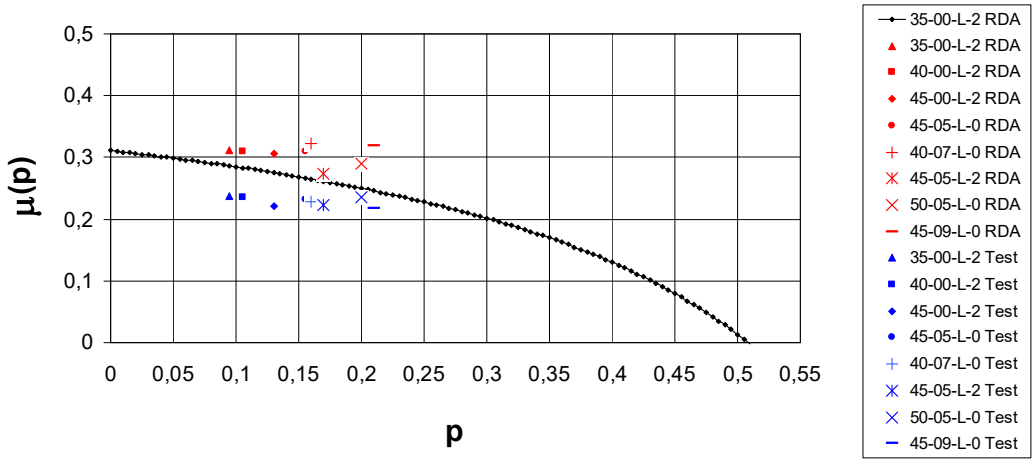

Figure 4. Comparison of tested and numerically calculated Poisson's ratios with functional dependence of Poisson's ratio versus porosity for sample No. 1 according to the RDA model

For all concrete samples except for sample No. 6 (45-05-L-2) an excellent agreement between the calculated and tested strengths is observed, [13]. Note that the calculated parameters were obtained using Poisson's ratios which are obtained from the P and S wave velocities.

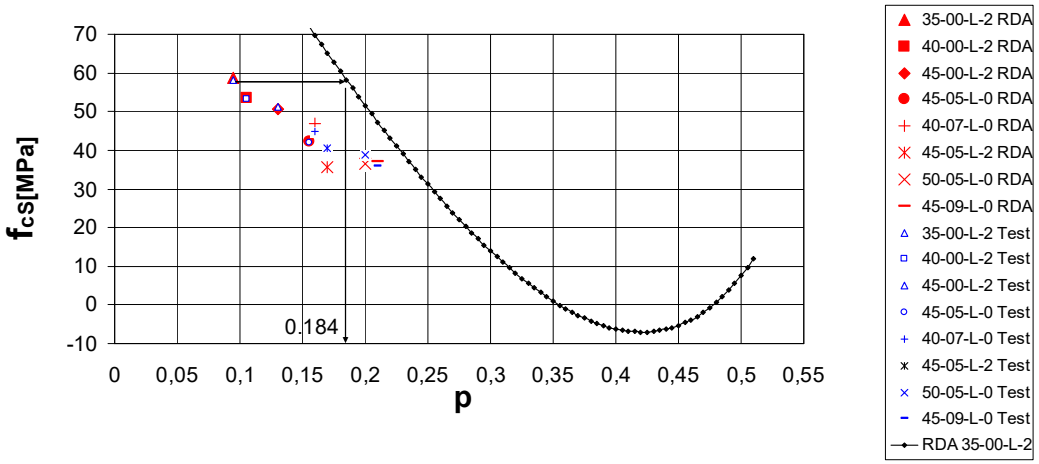

Figure 5. Comparisons of tested and calculated compressive strengths for established p_f, which control static strengths

The RDA method is based on a completely new concept of calculated VVF-s, based on the energy densities. The VVF-s control the static strengths, in contrast to all other models based on the measured porosities of unloaded samples described in detail in the work of [27]. Therefore, the measured porosity of sample 35-00-L-2 increase from 0.0944 to the value of 0.184. It can be argued that the difference of 0.0896 is the volume fraction of cracks.

It should be noted that the experimental compressive strengths f_{cS} were obtained for saturated samples only. The strengths of saturated sample are lower than the strengths of the dry samples. Therefore, strengths f_{cS} - not static strengths f_{US2} - are comparable to strengths σ_f.

The comparison of damage variables and dynamic strengths in [13] shows the validity of the proposed RDA model. Differences in damage variables are a consequence of the adopted spherical void shapes for calculating the variable D_{LD}. The differences between dynamic strengths f_{US1} and strengths σ_{min} controlled by minimum porosities is within reasonable limits.

5. ANALYSIS OF POROUS ROCK SAMPLES

Numerous versions of elasto-acoustic techniques have been developed to analyze the overall behavior of wave propagation in composite media. Theoretical models of composite materials have primarily been used for porous materials such as concrete, rock and ceramics, [27] and [28]. Among the different types of materials, rocks have an important place, due to their applications in various disciplines including the energy sector. In order to prove the validity of the proposed model, three different types of rocks were selected and analyzed: sandstone, granite and limestone.

The sandstone rock is presented as an author's research, [18]. The goal was to compare the calculation results with the measured values. The investigated rock is sandstone from the area of Bijeljina, which is located in the Republic of Srpska - Bosnia and Herzegovina.

Granite from HengYang region, China, was analyzed by Xiao et al. u [29], [30]. Based on experimental observations, the authors proposed a model of damage that can represent the whole process of damage due to fatigue.

Yasar and Erdogan in [31] analyzed carbonate rocks from several regions of Turkey. During sampling, unbedded rock types were selected to eliminate anisotropic effects on the measurements. Three different types of carbonate rocks were included in the research: dolomite, marble and limestone.

Figure 6 shows a comparison of the complete stress-strain curves for the analyzed rock samples obtained by the RDA model. The modulus of elasticity is the lowest for the limestone sample, while the highest for the granite.

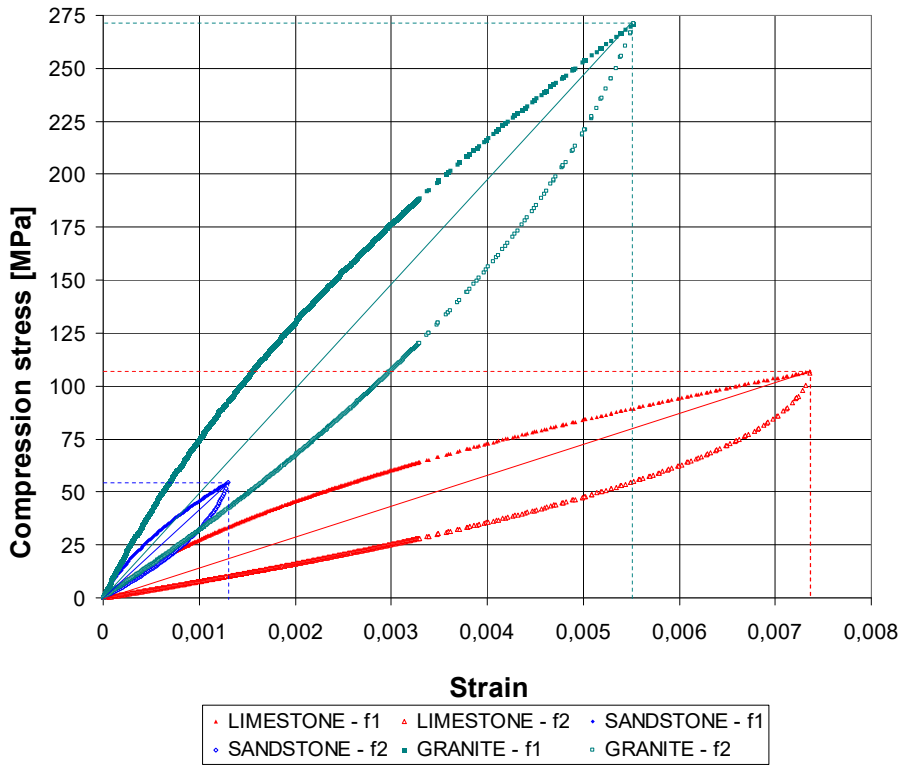

Figure 6. Dynamic stress-strain curves according to the RDA model for the analyzed rock samples

5.2. SANDSTONE ROCK SAMPLE

A cylindrical sample with a diameter of 73.5 mm was drilled from block B-1(I) (1.7 - 2.0 m) and cut to a length of 141.8 mm with a high-speed rotary saw. The end surfaces of the sample were ground with a grinder according to the standard. The measured density was 2526 kg/m3. The experiment was conducted on the PUN-DIT measuring equipment in the Material Testing Laboratory of the Technical Institute of Bijeljina. The complete stress-strain analysis was performed by [18] using the RDA method, whereby the UCS, as well as the dynamic f_{US1} and static f_{US2} strengths, were calculated considering only the measured velocities of P and S waves.
Table 1 shows the calculated energy densities and corresponding porosities. The last column shows the damage variable for the calculated porosity p_f. Based on the damage variable of 0.53 at zero porosity we can be concluded that it decreases to 0.42 due to porosity $p_f = 0.15$, which controls the static strength.

Table 1. RDA model parameters for the sandstone sample [18]

W_{el} [MJ/m^3]	W_{d1} [MJ/m^3]	W_{d2} [MJ/m^3]	p_{max}	p_E	p_f	D_f
0.035432	0.041678	0.026939	0.415972	0.176295	0.152368	0.415689

5.3. GRANITE ROCK SAMPLE

The FI-24 granite sample was cylindrical, 50 mm in diameter, and 100 mm in height. Experimental data for UCS and modulus of elasticity taken from Xiao et al. [29] were used in this paper. A complete stress-strain analysis was performed by Milašinović [18] using the RDA method, where dynamic f_{US1} and static f_{US2} strengths were calculated p_f. Table 2 shows the calculated energy densities and corresponding porosities. The last column shows the damage variable for calculated

p_f. Based on the damage variable of 0.47 at zero porosity can be concluded that it decreases to 0.36 due to the porosity $p_f = 0.13$.

Table 2. RDA model parameters for the granite sample [29]

W_{el} [MJ/m^3]	W_{d1} [MJ/m^3]	W_{d2} [MJ/m^3]	p_{max}	p_E	p_f	D_f
0.748141	0.86548	0.594703	0.361934	0.156842	0.133313	0.359524

5.4. LIMESTONE ROCK SAMPLE

Sound speed measurements were performed on five core samples with a diameter of 42 mm prepared in laboratory conditions. Conventionally, maximum, mean, and minimum velocities are found. The results of measured sound speeds and rock density (2430 kg/m^3), as well as empirically predicted Young's moduli and UCS of rocks are presented in [31]. Milašinović [18] performed a complete stress and deformation analysis of the selected sample of limestone, where the dynamic f_{US1} and static f_{US2} strengths were calculated. Table 3 shows the calculated energy densities and corresponding porosities. The last column shows the damage variable for the calculated porosity p_f which controls the static failure of the sample.

Table 3. RDA model parameters for the limestone sample, [31]

W_{el} [MJ/m^3]	W_{d1} [MJ/m^3]	W_{d2} [MJ/m^3]	p_{max}	p_E	p_f	D_f
0.390282	0.472888	0.26925	0.521772	0.211658	0.188698	0.526162

5.5. COMPARATIVE ANALYSIS OF POROUS DRY ROCK SAMPLES

The compressive strengths for the three analyzed rock samples are present in Table 4.

Table 4. Compressive strengths for the analyzed rock samples

Rock	E_H [MPa]	σ_{ef} [MPa]	UCS [MPa]	f_{US2} [MPa]	f_{test} [MPa]	σ_f [MPa]
Granite	49043	270.89	143.43	122.03	**114.75**	**110.03**
Limestone	14400	106.02	**38.7**	33.18	-	**39.94**
Sandstone	41831	54.45	25.65	**21.74**	-	**21.93**

The static strength f_{US2} agrees very well with the strength σ_f in the case of the sandstone sample with a proven VVF of $p_f = 0.15$. A possible reason for this is the fact that all the parameters of this sample as well as all the strengths were calculated using the measured velocities of P and S waves. The mass of the dry sample is determined by weighing, and the density by precise calculation of its volume. These results unequivocally confirm the correctness of the proposed RDA model.

For the granite sample, the difference between strength f_{US2} and strength σ_f is greater. However, in the work [29] authors reported that the sample had a maximum static strength of 114.75 MPa, which shows much better agreement with the 110 MPa strength calculated here. The modulus of elasticity was calculated from the stress-strain curve under static loading. The test was performed on an electro-hydraulic servo controlled rock testing machine RMT-150B, [30]. It is also important to point out that only the P-wave velocity is used to calculate the parameters of the RDA model in this paper. The density of the sample =2710 kg/m^3 is taken from the textbook [32] because the actual is not shown. Obviously, independent tests lead to differences in results, but they are within acceptable limits.

For the limestone rock sample, the difference between strength f_{US2} and strength σ_f is the largest. However, in the work [31] the authors stated that the two main parameters, modulus of elasticity and UCS, were empirically predicted. This is probably the reason why strength matches well with UCS rather than static strength f_{US2}.

Figure 7 shows the comparative results for the Poisson's ratios which show that the highest initial Poisson's ratio is for the limestone sample and the lowest for the granite sample.

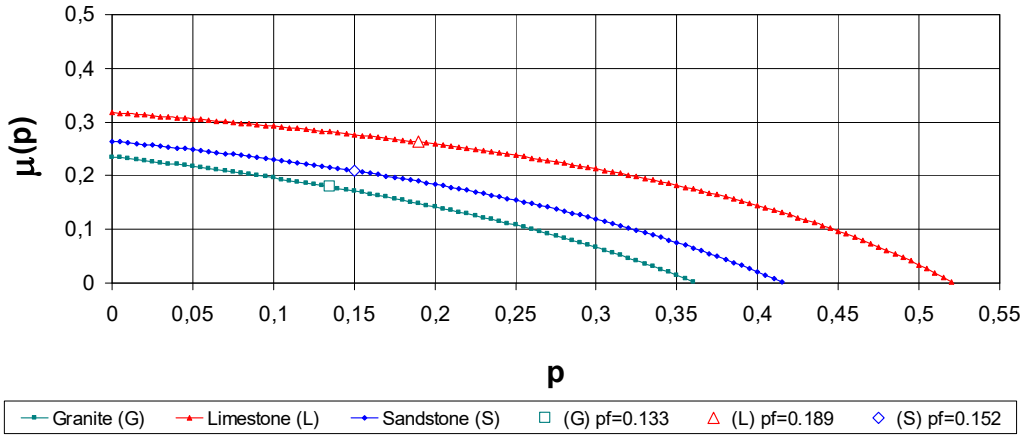

Figure 7. Poisson's ratios versus porosity for the analyzed rock samples

Figure 8 shows a significant decrease in strength with increasing porosity. However, although strength is a nonlinear function of porosity, in the range of measurable porosities an approximately linear decrease in strength with increasing porosity can be observed for all three analyzed samples. Although the porosities controlling the static strength are different, the strength drop to 0.4 from the effective stress is about the same.

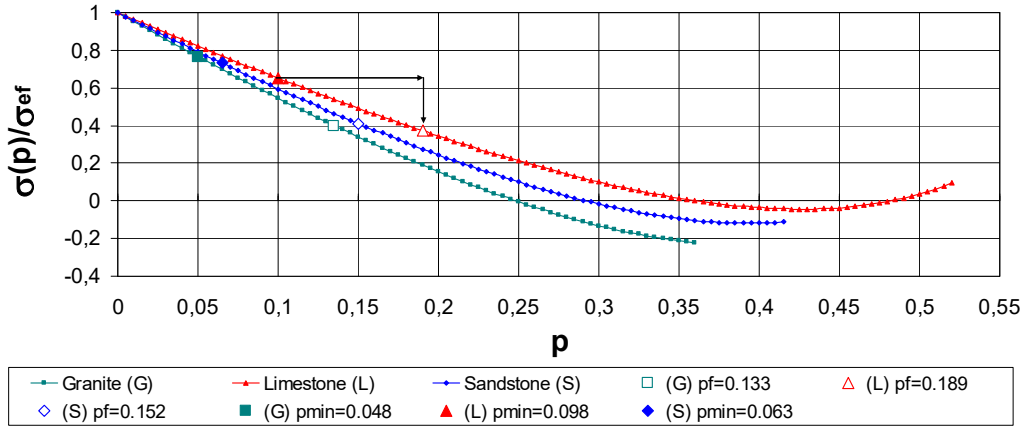

Figure 8. Dimensionless compressive strengths versus porosity for the analyzed rock samples

The results in this paper show that D_{LD} corresponds to reality only for p_{max} because in that case D_{LD} represents the damage variable D_1 from the RDA model, Table 5. Damage variables D_{LD} have slightly higher values due to the assumption of spherical voids that do not exist in the real materials. Table 5 shows comparisons of the dynamic strength f_{US1} with the strength σ_{min} controlled by the porosity p_{min}. Accordingly, the validity of the proposed RDA model is reconfirmed.

Table 5. Comparison of damage variables and dynamic strengths for the analyzed rock samples

Rock	D_1	p_{max}	$D_{LD} = p_{max}^{2/3}$	f_{US1} [MPa]	p_{min}	ρ_0 [kg/m^3]	σ_{min} [MPa]
Sandstone	**0.529**	0.416	**0.557**	**41.5**	0.063	2697	**40.2**
Granite	**0.471**	0.362	**0.508**	**213.1**	0.048	2847	**209.7**
Limestone	**0.635**	0.522	**0.648**	**76.3**	0.098	2695	**69.7**

Finally, based on the p_{min}, the initial density of rock sample at zero porosity $\rho_0 = \rho/1 - p_{min}$ can be determined, Table 5. The calculated initial densities correspond to the experimental ones, according to the textbook [32].
Table 6 shows dimensionless moduli of elasticity for the previously calculated porosities.

Table 6. Comparison of dimensionless moduli of elasticity for the analyzed rock samples

Rock	$E_{H,min}/E_{H,0}$	$E_{H,f}/E_{H,0}$	$E_{H,max}/E_{H,0}$
Sandstone rock sample	0.9199	0.8067	0.4711
Granite rock sample	0.9376	0.8271	0.5295
Limestone rock sample	0.8808	0.7701	0.365

Figure 9 shows dimensionless moduli of elasticity as a function of porosity for the analyzed rock samples.

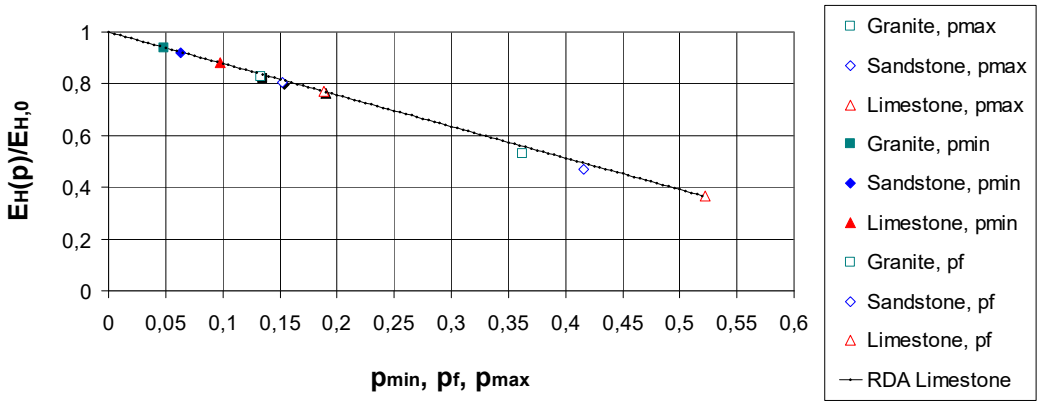

Figure 9. Dimensionless moduli of elasticity versus porosity for the analyzed rock samples

Comparison of the RDA law for modulus of elasticity as a function of porosity with experimental moduli obtained from P and S wave velocities shows excellent agreement of the results. The inclusion of damage variable in the law, shows that the modulus will not drop to zero even at maximum porosity. This fact in rock materials is real. If $D_1 = 1$, it is a break of the sample into two parts, which rarely happens.

6. CONCLUSIONS

The key result proposed in this paper refers to a new way of calculating porosities or VVF-s through energy densities. Results show that in all analyzed materials, VVF-s that control static strengths range from 0.14 to 0.25, which is in accordance with the research of [22] and [23]. The differences that appear in the calculated damage variables are due to the assumption of spherical voids in the Lemaitre and Dufailly [24] prediction that do not appear in actual damaged materials.
Yaman et al. [26], [27] found a valid model for predicting the modulus of elasticity of saturated concrete by comparing different methods, including micromechanical methods, experimental and semi-experimental methods, in which the Kuster-Toksoz [33] method was more effective than the others. The RDA method proposed in this paper gives excellent results for the analyzed hardened concretes analyzed by Yaman et al.
Of the three rock types analyzed in this paper, only the sandstone sample has fully defined RDA model parameters based on P and S wave velocities. The results show that the static strength agrees very well with the static strength obtained by the previously calculated porosity on the sample failure. This unequivocally confirms the correctness of the proposed model. For the granite sample, only the P-wave velocity was used, while the modulus of elasticity and UCS were taken from statically independent tests. This led to differences in the results, but they are within acceptable limits. Empirically estimated mechanical properties, including strength, were taken for the limestone sample. In this case, the strength obtained by the previously calculated porosity on the sample failure

agrees satisfactorily with the UCS of the sample. Finally, the initial density for the analyzed rock samples at zero porosity is determined based on the porosity p_{min}.

LITERATURE

[1] J. A. Choren, S. M. Heinrich, and M. B. Silver-Thorn, "Young's modulus and volume porosity relationships for additive manufacturing applications," *Journal of Materials Science*, vol. 48, no. 15. pp. 5103–5112, Aug. 2013, doi: 10.1007/s10853-013-7237-5.

[2] R. M. Spriggs, "Expression for Effect of Porosity on Elastic Modulus of Polycrystalline Refractory Materials, Particularly Aluminum Oxide," *J. Am. Ceram. Soc.*, vol. 44, no. 12, pp. 628–629, Dec. 1961, doi: 10.1111/J.1151-2916.1961.TB11671.X.

[3] E. Ryshkewitch, "Compression Strength of Porous Sintered Alumina and Zirconia," *J. Am. Ceram. Soc.*, vol. 36, no. 2, pp. 65–68, Feb. 1953, doi: 10.1111/J.1151-2916.1953.TB12837.X.

[4] K. K. Phani and S. K. Niyogi, "Young's modulus of porous brittle solids," *J. Mater. Sci. 1987 221*, vol. 22, no. 1, pp. 257–263, Jan. 1987, doi: 10.1007/BF01160581.

[5] J. C. Wang, "Young's modulus of porous materials," *J. Mater. Sci.*, vol. 19, no. 3, pp. 801–808, Mar. 1984, doi: 10.1007/BF00540451.

[6] A. M. Neville and J. J. Brooks, *Concrete technology*. Pearson Education Limited, 2010.

[7] X. Chen, S. Wu, and J. Zhou, "Influence of porosity on compressive and tensile strength of cement mortar," *Constr. Build. Mater.*, vol. 40, pp. 869–874, Mar. 2013, doi: 10.1016/J.CONBUILDMAT.2012.11.072.

[8] X. Chen, D. Shi, and S. Guo, "Experimental Study on Damage Evaluation, Pore Structure and Impact Tensile Behavior of 10-Year-Old Concrete Cores After Exposure to High Temperatures," *Int. J. Concr. Struct. Mater.*, vol. 14, no. 1, pp. 1–17, Mar. 2020, doi: 10.1186/s40069-020-0393-5.

[9] R. Kumar and B. Bhattacharjee, "Porosity, pore size distribution and in situ strength of concrete," *Cem. Concr. Res.*, vol. 33, no. 1, pp. 155–164, Jan. 2003, doi: 10.1016/S0008-8846(02)00942-0.

[10] O. AlShareedah and S. Nassiri, "Pervious concrete mixture optimization, physical, and mechanical properties and pavement design: A review," *J. Clean. Prod.*, vol. 288, p. 125095, Mar. 2021, doi: 10.1016/J.JCLEPRO.2020.125095.

[11] R. W. Zimmerman, *Compressibility of sandstones*. Amsterdam: Elsevier, 1991.

[12] F. Gassmann, "Elastic Waves through a Packing of Spheres," *Geophysics*, vol. 16, no. 4, pp. 673–685, Mar. 1951, doi: 10.1190/1.1437718.

[13] D. D. Milašinović, "Modeling of porous-hardened concrete by rheological-dynamical analogy," *Eng. Comput. (Swansea, Wales)*, vol. 40, no. 9/10, pp. 2615–2647, Dec. 2023, doi: 10.1108/EC-08-2022-0574/FULL/XML.

[14] D. D. Milašinović, "Rheological-dynamical continuum damage model for concrete under uniaxial compression and its experimental verification," *Theor. Appl. Mech.*, vol. 42, no. 2, pp. 73–110, 2015, doi: 10.2298/tam1502073m.

[15] D. Milašinović, D. Goleš, A. Rožnjik, and N. M. Bošnjak, "Model of porous materials by rheological-dynamical analogy using the principles of mass and energy conservation," *Int. Conf. Contemp. Theory Pract. Constr. / Међународна конференција Савремена теорија и пракса у градитељству*, no. 15, pp. 092–103, Jun. 2022, doi: 10.7251/STP2215092M.

[16] J. Lemaitre, A Course on Damage Mechanics. 1992.

[17] D. D. Milašinović, D. Majstorović, and R. Vukomanović, "Quasi static and dynamic inelastic buckling and failure of folded-plate structures by a full-energy finite strip method," *Adv. Eng. Softw.*, vol. 117, pp. 136–152, Mar. 2018, doi: 10.1016/j.advengsoft.2017.07.013.

[18] D. D. Milašinović, "Rheological-dynamical method for prediction of compressive strength and deformation of rocks," *Int. J. Rock Mech. Min. Sci.*, vol. 141, p. 104659, May 2021, doi: 10.1016/j.ijrmms.2021.104659.

[19] S. Murakami, *Continuum Damage Mechanics*, vol. 185. Dordrecht: Springer Netherlands, 2012.

[20] A. L. Gurson, "Continuum theory of ductile rupture by void nucleation and growth - 1. yield criteria and flow rules for porous ductile media.," *Am. Soc. Mech. Eng.*, no. 76-Mat-CC, 1976.

[21] G. Rousselier, "Ductile fracture models and their potential in local approach of fracture," *Nucl. Eng. Des.*, vol. 105, no. 1, pp. 97–111, Dec. 1987, doi: 10.1016/0029-5493(87)90234-2.

[22] S. H. Goods and L. M. Brown, "Overview No. 1: The nucleation of cavities by plastic deformation," *Acta Metall.*, vol. 27, no. 1, pp. 1–15, Jan. 1979, doi: 10.1016/0001-6160(79)90051-8.

[23] A. Needleman and V. Tvergaard, “An analysis of ductile rupture in notched bars,” *J. Mech. Phys. Solids*, vol. 32, no. 6, pp. 461–490, Jan. 1984, doi: 10.1016/0022-5096(84)90031-0.
[24] J. Lemaitre and J. Dufailly, “Damage measurements,” *Eng. Fract. Mech.*, vol. 28, no. 5–6, pp. 643–661, Jan. 1987, doi: 10.1016/0013-7944(87)90059-2.
[25] D. D. Milašinović, “Rheological–dynamical analogy: visco-elasto-plastic behavior of metallic bars,” *Int. J. Solids Struct.*, vol. 41, no. 16–17, pp. 4599–4634, Aug. 2004, doi: 10.1016/j.ijsolstr.2004.02.061.
[26] I. O. Yaman, N. Hearn, and H. M. Aktan, “Active and non-active porosity in concrete. Part I: Experimental evidence,” *Mater. Struct. Constr.*, vol. 34, no. 246, pp. 102–109, 2002, doi: 10.1007/BF02482109.
[27] I. O. Yaman, H. M. Aktan, and N. Hearn, “Active and non-active porosity in concrete Part II: Evaluation of existing models,” *Mater. Struct. 2002 352*, vol. 35, no. 2, pp. 110–116, 2002, doi: 10.1007/BF02482110.
[28] R. W. Zimmerman, “Elastic moduli of a solid containing spherical inclusions,” *Mech. Mater.*, vol. 12, no. 1, pp. 17–24, Aug. 1991, doi: 10.1016/0167-6636(91)90049-6.
[29] J. Q. Xiao, D. X. Ding, G. Xu, and F. L. Jiang, “Inverted S-shaped model for nonlinear fatigue damage of rock,” *Int. J. Rock Mech. Min. Sci.*, vol. 46, no. 3, pp. 643–648, Apr. 2009, doi: 10.1016/J.IJRMMS.2008.11.002.
[30] J. Q. Xiao, D. X. Ding, F. L. Jiang, and G. Xu, “Fatigue damage variable and evolution of rock subjected to cyclic loading,” *Int. J. Rock Mech. Min. Sci.*, vol. 47, no. 3, pp. 461–468, Apr. 2010, doi: 10.1016/J.IJRMMS.2009.11.003.
[31] E. Yasar and Y. Erdogan, “Correlating sound velocity with the density, compressive strength and Young’s modulus of carbonate rocks,” *Int. J. Rock Mech. Min. Sci.*, vol. 41, no. 5, pp. 871–875, Jul. 2004, doi: 10.1016/J.IJRMMS.2004.01.012.
[32] J. C. Jaeger, N. G. W. Cook, and R. W. Zimmerman, *Fundamentals of rock mechanics - Fourth edition*, vol. 38, no. 3–4. 2007.
[33] G. T. Kuster and M. N. Toksoz, “Velocity and attenuation of seismic waves in two-phase media: Part I. Theoretical formulations,” *Geophysics*, vol. 39, no. 5, pp. 587–606, Feb. 2012, doi: 10.1190/1.1440450.